NASA TECHNICAL NOTE

NASA TN D-4678

NASA TN D-4678

WIND-TUNNEL CALIBRATION OF A 40° CONICAL PRESSURE PROBE AT MACH NUMBERS FROM 3.5 TO 7.4

by Frank W. Burcham, Jr.

Flight Research Center
Edwards, Calif.

NATIONAL AERONAUTICS AND SPACE ADMINISTRATION • WASHINGTON, D. C. • JULY 1968

NASA TN D-4678

WIND-TUNNEL CALIBRATION OF A 40° CONICAL PRESSURE PROBE AT MACH NUMBERS FROM 3.5 TO 7.4

By Frank W. Burcham, Jr.

Flight Research Center
Edwards, Calif.

NATIONAL AERONAUTICS AND SPACE ADMINISTRATION

For sale by the Clearinghouse for Federal Scientific and Technical Information
Springfield, Virginia 22151 – CFSTI price $3.00

WIND-TUNNEL CALIBRATION OF A 40° CONICAL PRESSURE PROBE AT MACH NUMBERS FROM 3.5 TO 7.4

By Frank W. Burcham, Jr.
Flight Research Center

SUMMARY

A wind-tunnel calibration of a 40° included-angle flow-field cone probe was made over a Mach number range of 3.5 to 7.4. The cone probe was designed and fabricated by the NASA Flight Research Center to obtain flow-field data on the X-15 airplane. Estimated accuracy of the calibration was ±2 percent in Mach number and ±0.2° in flow angularity at a Mach number of 7.4. Reynolds number effects were negligible over the test range of 0.65 million to 3.25 million per foot (0.20 million to 1.0 million per meter). A rake designed for flight on the X-15 was used to mount two cone probes. Slightly different calibrations resulted for the two cones because of differences in the cone afterbody configurations.

INTRODUCTION

A conical pressure probe for surveying the flow field beneath the fuselage of an X-15 aircraft has been developed by the NASA Flight Research Center. The flow field in this region is of interest because of the possibility of mounting an airbreathing engine on the X-15 and flight testing it over the Mach number range of 3 to 8 (ref. 1). Design and operation of the engine and evaluation of its performance would require a knowledge of the flow-field Mach number, total, static, and dynamic pressure, and flow angularity. Since these parameters vary considerably with free-stream Mach number and angle of attack, wind-tunnel and theoretical studies (refs. 2 to 4) of the flow field were performed. However, full-scale flight data are also desirable.

Previous studies (refs. 5 to 7) showed the feasibility of using conical pressure probes for surveying flow fields. The cones used in these investigations were designed for wind-tunnel testing and so were small in order to minimize flow disturbances. Also, to minimize pressure lag, pressure orifices on the cones needed to be as large as possible. As a result, the cones were small with relatively large orifices, which caused the cone probes to deviate from a sharp-cone theoretical calibration. The small size of the cones also made accurate fabrication difficult.

For use on the X-15 airplane, a small cone was not essential. Therefore, a relatively large 40° included-angle cone probe was developed to minimize the undesirable characteristics of smaller cones and to permit easy and accurate fabrication. This paper presents results of the calibration tests performed at the NASA Ames Research Center. Tests were made over the Mach number range from 3.5 to 7.4.

Reynolds numbers ranged from 0.65×10^6 to 3.25×10^6 per foot (0.20×10^6 to 1.0×10^6 per meter). The angle-of-attack range was -2° to 10°. Since only small sidewash angles are expected in the X-15 flow field (ref. 2), the calibrations were performed mainly in the pitch plane.

SYMBOLS

The units used for the physical quantities in this paper are given in U. S. Customary Units and parenthetically in the International System of Units (SI). Factors relating the two systems are presented in reference 8.

M_1 — Mach number ahead of normal shock wave at cone apex (local-stream Mach number)

N_{Re} — Reynolds number, per foot (per meter)

$\bar{p}_A$ — arithmetic mean of four cone surface static pressures, $\frac{1}{4}(p_{s,a} + p_{s,b} + p_{s,c} + p_{s,d})$, lb/sq ft (kN/sq m)

p_s — cone surface static pressure, lb/sq ft (kN/sq m)

$p_{t,1}$ — total pressure ahead of normal shock wave at cone apex (local-stream total pressure), lb/sq ft or lb/sq in. (kN/sq m)

$p_{t,2}$ — total pressure measured behind normal shock wave at cone apex (impact pressure), lb/sq ft (kN/sq m)

p_1 — static pressure ahead of normal shock wave at cone apex (local-stream static pressure), lb/sq ft (kN/sq m)

$\frac{\Delta p}{q_1}$ — pressure-difference coefficient

$\left(\frac{\Delta p}{q_1}\right)_\alpha = \frac{p_{s,c} - p_{s,a}}{q_1}$ (see fig. 1)

$\left(\frac{\Delta p}{q_1}\right)_\beta = \frac{p_{s,b} - p_{s,d}}{q_1}$ (see fig. 1)

q_1	dynamic pressure ahead of normal shock wave at cone apex (local-stream dynamic pressure), lb/sq ft (kN/sq m)
α	angle of attack, deg
β	angle of sideslip, deg

Subscripts:

a,b,c,d	position of surface static orifices on cone (see fig. 1)
α	quantity at angle of attack
α=0	quantity at zero angle of attack

DESCRIPTION OF CONE PROBES

A drawing of the 40° included-angle cone probe is shown in figure 1. The cone has a nose impact-pressure orifice with a sharp edge. Four surface static-pressure

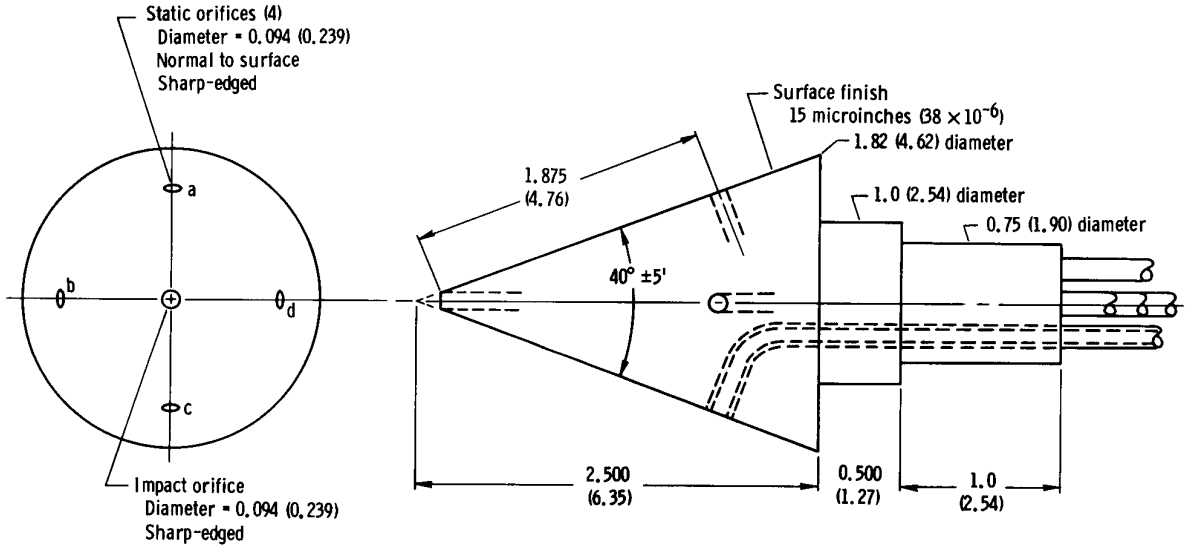

Figure 1.– Drawing of 40° included-angle cone probe. Dimensions in inches (centimeters) unless otherwise noted.

orifices are positioned 90° apart. These four orifices are normal to the surface, sharp-edged, and about 20 orifice diameters from the nose impact orifice. The surface finish is as smooth as practical, averaging about 15 microinches (38×10^{-6} centimeters). The cones tested were fabricated from Inconel X. This material was used because of its ability to withstand the temperatures expected on X-15 flights to Mach numbers above 7.

To enlarge the flow region being investigated on the X-15 during a flight, two cone probes would be used at the same time, thus allowing the desired test data to be obtained with fewer flights. For this purpose, a rake was designed to accommodate a cone probe at two locations. Figure 2 shows the rake, which was made of Inconel, with two cones attached. The angular position of this rake is ground adjustable to any of the six angular positions shown. Thus, the center cone remains fixed, while the outer cone can be moved to survey different areas.

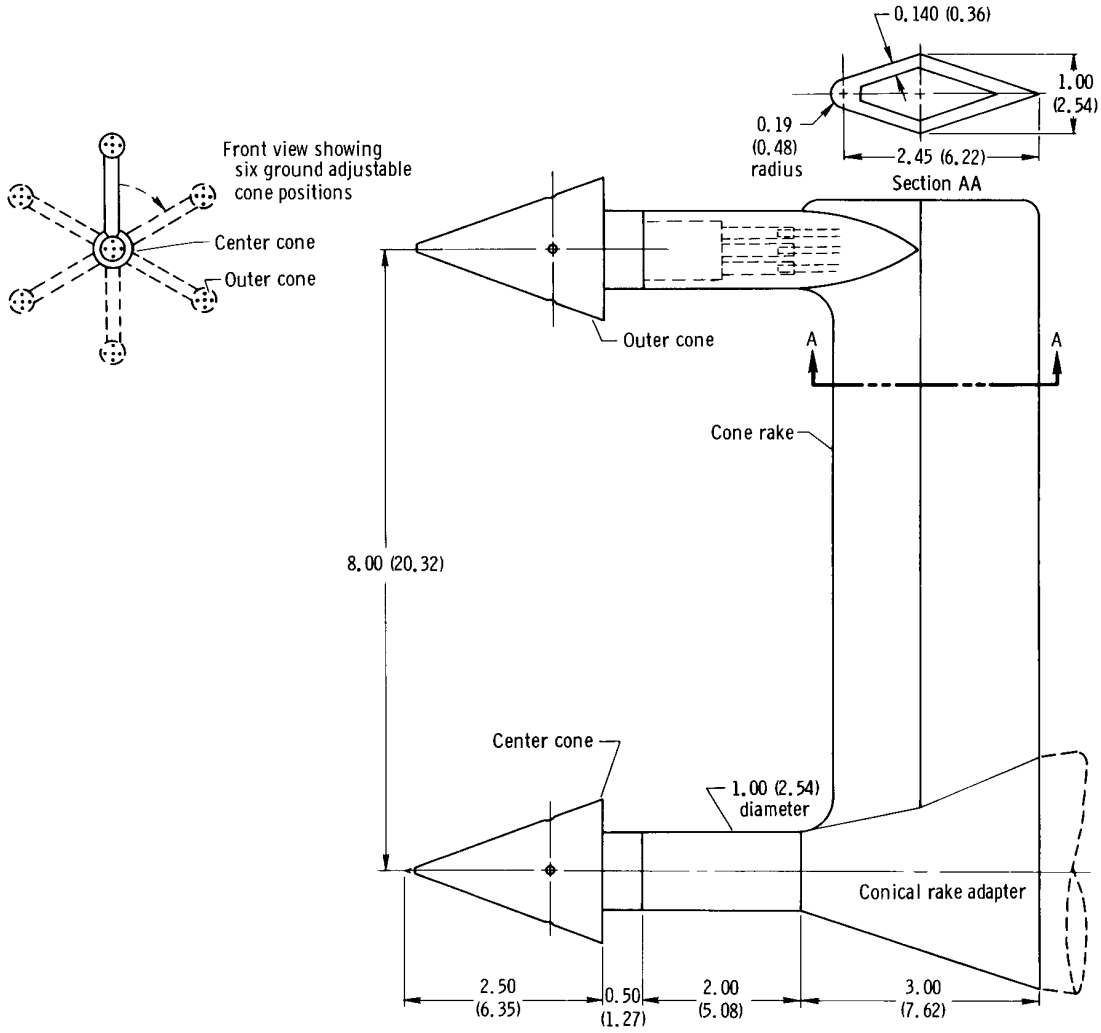

Figure 2.– Drawing of rake with two cone probes. All dimensions in inches (centimeters) unless otherwise noted.

For high Mach number flights, the leading edge of the rake would be thermally protected by a molded ablative coating to prevent warpage of the rake due to temperature gradients, with a consequent angular displacement of the outer cone. Figure 3 is a photograph of the cone probes with the ablative coating on the rake leading edge. To avoid using ablative materials in the wind tunnels, a steel bar (fig. 4) that closely simulated the molded ablative coating was constructed and used in some of the wind-tunnel tests.

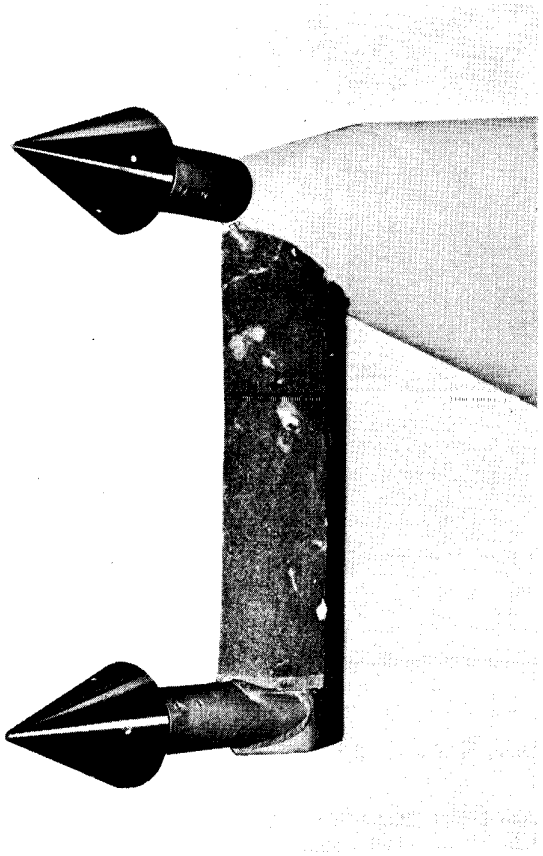

Figure 3.– Photograph of 40° cone probe rake with molded ablative coating on rake leading edge.

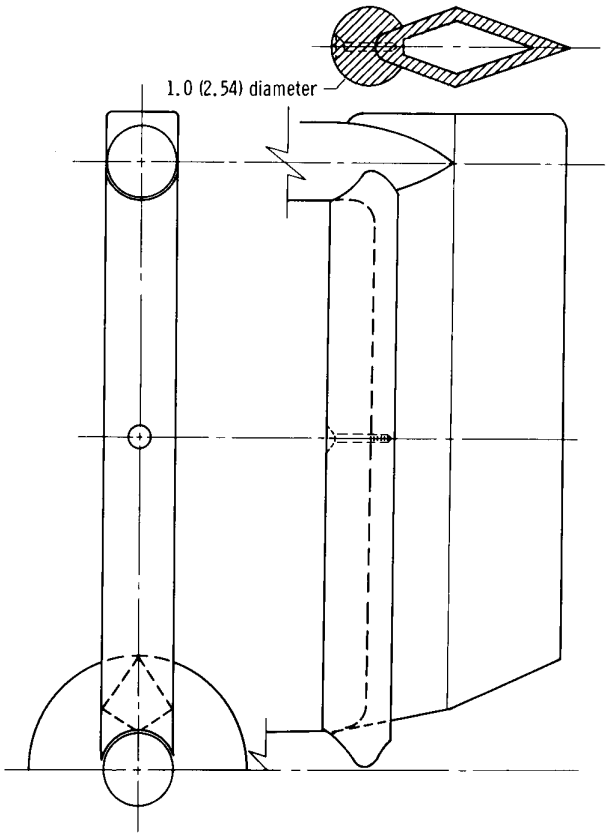

Figure 4.– Ablative simulator bar attached to rake leading edge.

TESTS

The calibrations were conducted in the NASA Ames Research Center's 1- by 3-Foot (30.5- by 91.4-centimeter) Supersonic Wind Tunnel, followed by tests in the 3.5-Foot (106.7-centimeter) Hypersonic Wind Tunnel. Test conditions were planned to cover the expected Mach/Reynolds number envelope for the X-15 and to permit testing at calibrated wind-tunnel conditions where minimum flow gradients existed. Figure 5 shows these test Reynolds numbers and Mach numbers superimposed on the X-15 flight envelope.

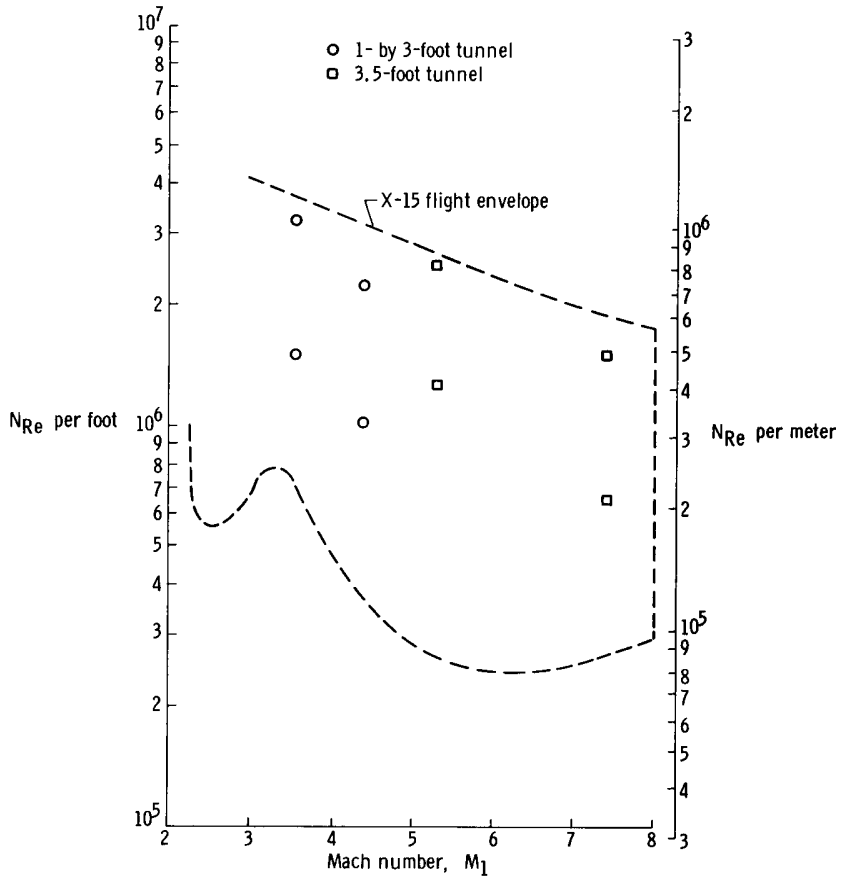

Figure 5.– Wind-tunnel calibration test conditions.

1- By 3-Foot Supersonic Wind Tunnel

The test conditions in the 1- by 3-foot tunnel are shown in the table below. This tunnel is a two-dimensional continuous-operation type with stagnation temperatures of approximately 550° R (306° K).

TEST CONDITIONS IN 1- BY 3-FOOT SUPERSONIC WIND TUNNEL

Run number	Nominal values				α, deg	β, deg	Configuration (see fig. 6)
	M_1	N_{Re} per ft $\times 10^{-6}$ (per m $\times 10^{-6}$)	$p_{t,1}$, lb/sq in. (kN/m^2)	q_1, lb/sq ft (kN/m^2)			
1	3.52	1.51 (0.46)	12 (8.27)	191 (9.15)	-2, 0, 1, 2, 3, 4, 6, 10, 0	0	B
2	3.52	3.25 (.99)	28 (19.31)	445 (21.31)			
3	4.38	2.25 (.69)	28 (19.31)	218 (10.44)			
4	4.38	1.00 (.30)	13 (8.96)	101 (4.84)			
5	3.52	1.51 (.46)	12 (8.27)	191 (9.15)			C
6	3.52	3.25 (.99)	28 (19.31)	445 (21.31)			
7	4.39	2.25 (.69)	28 (19.31)	218 (10.44)			
8	4.39	1.00 (.30)	13 (8.96)	101 (4.84)			

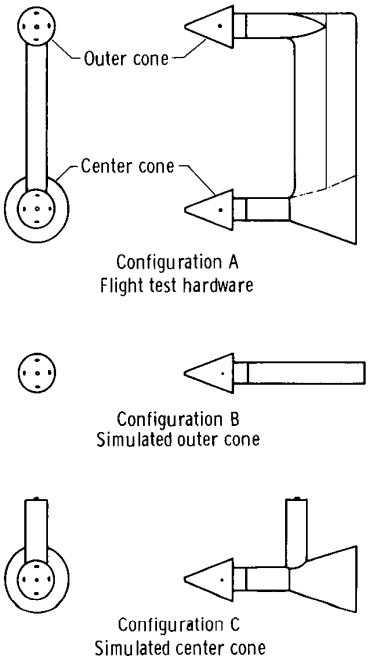

Figure 6.– Test configurations.

It had been planned to test the actual flight hardware in the tunnel (configuration A, fig. 6); however, to avoid possible interference effects between the two-cone rake and the 1- by 3-foot test section, it was decided to test a single-cone probe. Because the two cones have different downstream configurations (figs. 2 and 3), it was believed that both configurations should be tested. Thus, as shown in figure 6, a simulated outer cone (configuration B) and a simulated center cone (configuration C) were tested. Configuration B duplicated the outer-cone configuration of the rake except that the rake leading edge was not simulated because its afterbody effect was relatively small. For configuration C, however, the afterbody effect of the conical rake adapter was much larger and therefore was simulated. A cylindrical rod was used to simulate the molded ablative coating on the rake leading edge. A photograph of test configuration C is shown in figure 7.

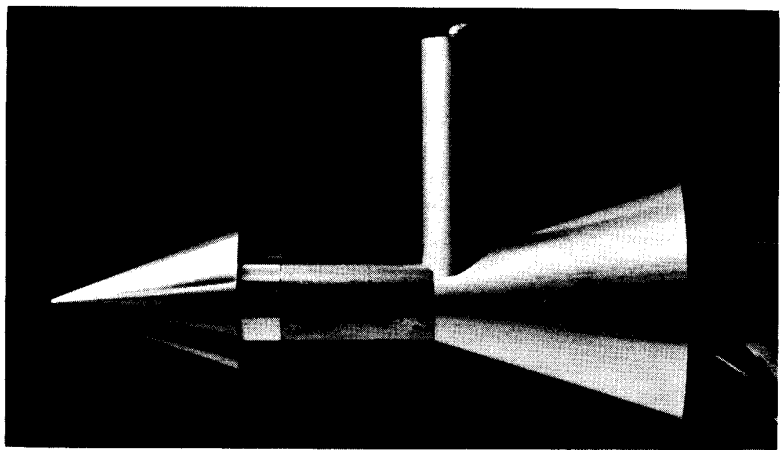

Figure 7.– Photograph of simulated center cone (configuration C) in 1- by 3-Foot Supersonic Wind Tunnel.

During the tests, data were recorded on a paper tape once for each test condition. These tapes were later processed and the output recorded on magnetic tape. Shadowgraphs were taken during each run.

3.5-Foot Hypersonic Wind Tunnel

The test conditions in the 3.5-foot tunnel are shown in the following table. This axisymmetric blow-down tunnel utilizes a pebble-bed heater to achieve stagnation

temperatures near 2000° R (1110° K). The flight hardware (configuration A) was tested in this tunnel. The ablative simulator bar (fig. 4) was added for two runs to determine its effect. Also for two runs, the cone rake was rotated 180° about the center cone (fig. 2) and the entire rake and its support mechanism were translated to effectively exchange the position of the two cones. This allowed a check to be made on the tunnel flow-angularity calibration and the symmetry of the cones. The cone probes had a polished surface before the tests; however, dust from the pebble-bed heater caused abrasion and pitting of the cone surface. Tests were made first at $M_1 = 7.4$ because the dusting was less severe than at $M_1 = 5.3$.

TEST CONDITIONS IN 3.5-FOOT HYPERSONIC WIND TUNNEL

Run number	Nominal values				α, deg (approximate)	β, deg	Configuration (see fig. 6)
	M_1	N_{Re} per ft $\times 10^{-6}$ (per m $\times 10^{-6}$)	$p_{t,1}$, lb/sq in. (kN/m^2)	q_1, lb/sq ft (kN/m^2)			
1	7.4	0.65 (0.20)	200 (137.90)	198 (9.48)	-2, 0, 1, 2, 3, 4, 6, 10, 0	0	A
2	7.4	.65 (.20)	200 (137.90)	198 (9.48)		0	A
3	7.4	1.50 (.46)	500 (344.74)	496 (23.75)		0	A
4	7.4	1.50 (.46)	500 (344.74)	496 (23.75)		0	(a)
5	7.4	1.50 (.46)	500 (344.74)	496 (23.75)		0	A, with ablative simulator
6	7.4	1.50 (.46)	500 (344.74)	496 (23.75)		-2	A
7	7.4	.65 (.20)	200 (137.90)	198 (9.48)		-2	A
8	5.3	1.25 (.38)	200 (137.90)	760 (36.39)		-2	A
9	5.3	1.25 (.38)	200 (137.90)	760 (36.39)		0	A
10	5.3	2.50 (.76)	400 (275.79)	1519 (72.73)		0	A
11	5.3	2.50 (.76)	400 (275.79)	1519 (72.73)		-2	A
12	5.3	2.50 (.76)	400 (275.79)	1519 (72.73)		-2	A, with ablative simulator
13	5.3	2.50 (.76)	400 (275.79)	1519 (72.73)	0	0	(a)

(a)Rake rotated 180° about center cone and translated.

Data were recorded five times at 2-second intervals for each test condition during a run in order to detect any fluctuations in cone pressures resulting from unsteady tunnel conditions. The data were recorded on magnetic tape which was later processed in a program that included real-gas effects. Shadowgraphs were taken during each run.

INSTRUMENTATION

1- By 3-Foot Supersonic Wind Tunnel

For tests in the 1- by 3-foot tunnel, variable-capacitance transducers were used to measure the five cone pressures. Seven of these transducers were set up to permit their simultaneous calibration, as shown in figure 8. The transducers were calibrated immediately before the first run, and zero settings were adjusted before each run. The reference side of the transducers was pumped down to a very low pressure, which was measured with a McLeod gage for both calibration and tests.

Differential-pressure transducers with a range of 0 to 1440 lb/sq ft (0 to 68.9 kN/m^2) were used to measure the impact pressure and the top and bottom static pressures. Differential-pressure transducers of 0 to 278 lb/sq ft (0 to 13.3 kN/m^2) were used to measure the two side static pressures. Quoted accuracy of the transducers was within 1 percent of full scale.

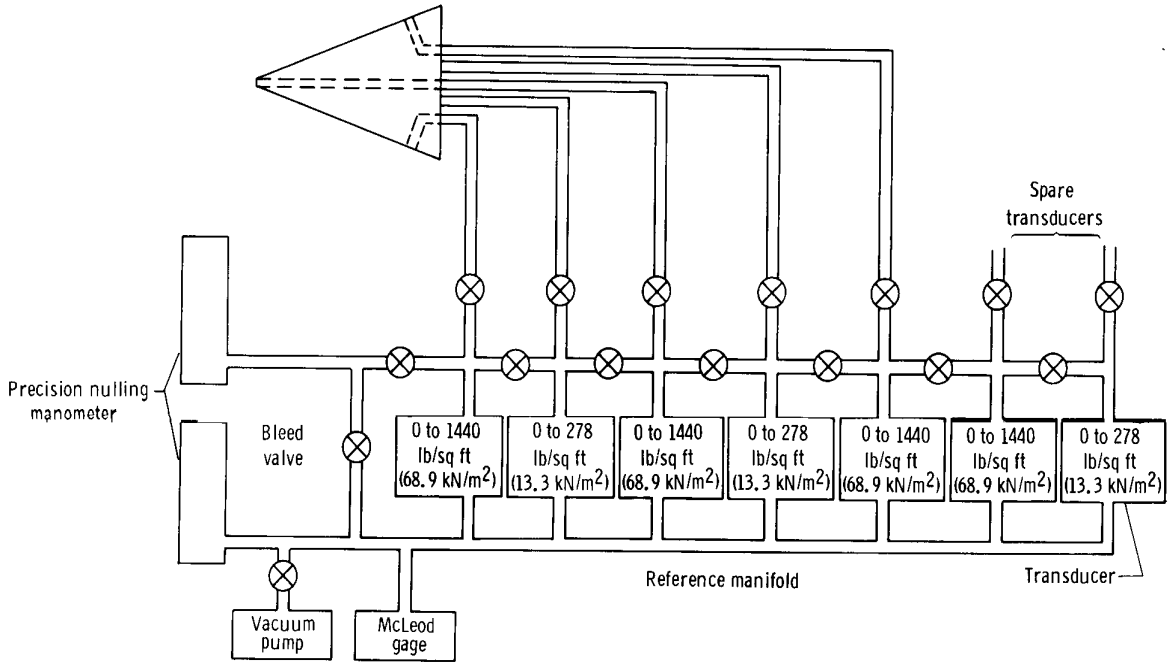

Figure 8.– Schematic drawing of pressure-sensing and calibrating system used in 1- by 3-Foot Supersonic Tunnel.

3.5-Foot Hypersonic Wind Tunnel

Tests in the 3.5-foot tunnel were conducted using the standard tunnel pressure-measurement system. This system consisted of 0 to 720, 0 to 1440, and 0 to 7200 lb/sq ft (0 to 34.4, 0 to 68.9, and 0 to 344.7 kN/m^2) absolute-pressure and ±360 lb/sq ft (±17.2 kN/m^2) differential-pressure miniature transducers. The differential-pressure transducers were connected across opposite pairs of cone static-pressure ports for comparison with the absolute-pressure transducers. Quoted accuracy of the transducers was ±2 percent of full scale. Zero corrections for these transducers were made immediately before each run.

ACCURACY

The absolute accuracy of the calibrations is difficult to establish because of the combined effects of many error sources. Care was taken during the calibrations to eliminate or minimize these error sources.

Four potential sources of bias error were investigated:

1. Fabrication accuracy of the cone probe

2. Alinement of the cone in the wind tunnel

3. Impact-pressure measurement

4. Surface pressure measurement

The first two sources of error were effectively eliminated. A study of the tolerances of three cones fabricated at the Flight Research Center indicated that differences noted would not be discernible because of the resolution of the pressure-sensing system. Alinement of the cone probe in the wind tunnel was carefully checked before each run and was verified by shadowgraphs. No error could be found, although shadowgraph angles could be determined only within ±0.2°.

The cone impact pressure was checked by assuming that the tunnel stagnation pressure and test section Mach number were accurate and by using normal shock theory to calculate the cone impact pressure. This comparison was extremely close at Mach numbers of 3.5 and 4.4 and within 0.5 percent at Mach numbers of 5.3 and 7.4.

The accuracy of the cone surface pressure was best assessed at zero angle of attack, where all four pressures should be equal. Generally, these pressures agreed within 0.5 percent. The probability of all four transducers having a similar bias error is small.

A source of uncertainty that could not be evaluated in the tests was the test section Mach number. Calibrations of the test section Mach number in the 1- by 3-foot tunnel are estimated to be accurate to ±0.005 in Mach number. In the 3.5-foot tunnel the accuracy is estimated to be ±0.03 in Mach number.

Since the bias errors are judged to be very small, the observed scatter in the data can be used as an indication of the random error. The following table represents the estimated accuracy of the data on the basis of the small bias error and the unfaired data scatter. Compressible flow theory (ref. 9) was used to calculate these parameters.

Flow-field parameter	Estimated accuracy			
	Nominal Mach number			
	3.5	4.4	5.3	7.4
	Percent			
M_1	±0.4	±0.6	±1.5	±2.0
$p_{t,1}$	±1.0	±2.0	±5.8	±8.4
p_1	±0.6	±0.8	±2.4	±3.4
q_1	±0.2	±0.3	±0.6	±0.4
	Degrees			
α, β	±0.1	±0.1	±0.2	±0.2

RESULTS AND DISCUSSION

The variation of the cone surface static-to-impact-pressure ratio $\frac{\bar{p}_A}{p_{t,2}}$ with Mach number for 0° angle of attack is shown in figures 9(a) and 9(b). The data agree with inviscid sharp-cone theory (ref. 10) at $M_1 = 3.5$ but are about 2 percent below theory for the three higher Mach numbers. Since there is no reason to suspect that the impact pressure $p_{t,2}$ would deviate from a theoretical value, it appears that the surface pressure $\bar{p}_A$ is lower than the theoretical sharp-cone value at the three higher test Mach numbers. A previous investigation (ref. 11) showed that the flow around a blunted cone overexpands near the nose to a surface pressure below the sharp-cone value. However, for the present tests, the orifices on the cones were positioned well downstream (20 impact-orifice diameters) in order to minimize or eliminate this effect. It seems more likely that the lower surface pressure may be the result of the upstream influence of the cone base pressure. Reference 12 discusses this effect. Theoretical and limited experimental studies indicate that the lower cone base pressure is able to propagate upstream through the subsonic portion of a laminar boundary layer a distance equal to many boundary-layer thicknesses. This would result in lower cone surface pressures near the trailing edge of the cone, as observed in the present tests.

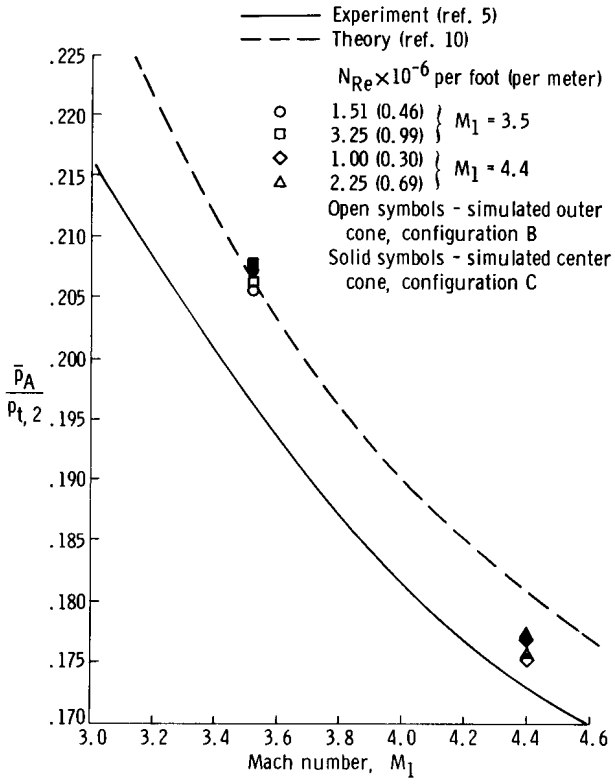

(a) 1- by 3-Foot Supersonic Wind Tunnel.

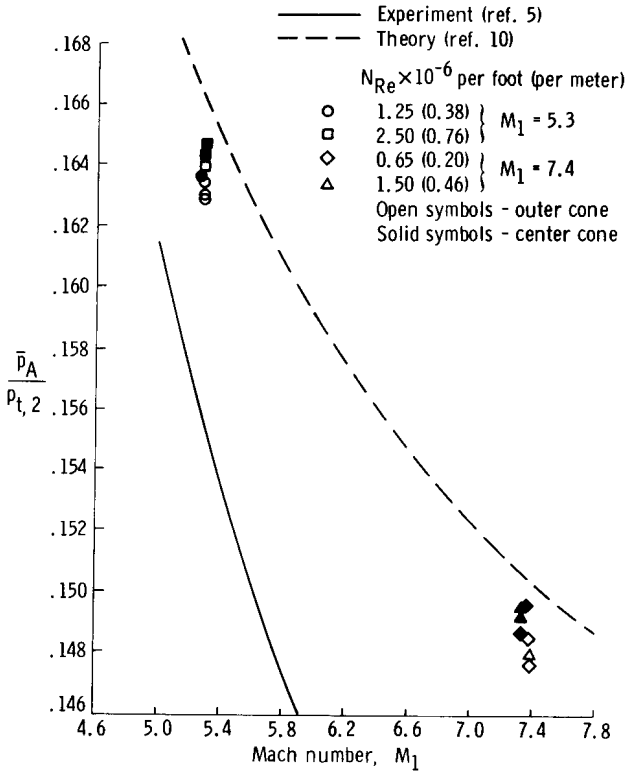

(b) 3.5-Foot Hypersonic Wind Tunnel; configuration A.

Figure 9.– Variation of average surface static-to-impact-pressure ratio with Mach number at 0° angle of attack.

Also included in figure 9 are experimental results for a similar 40° blunted-cone probe (ref. 5). For this smaller (diameter = 0.5 in. (1.27 cm)) cone the static orifices are only 8.5 impact-orifice diameters downstream. The overexpansion effect mentioned previously may explain why the static-to-impact-pressure ratio for this cone is lower than the theoretical value.

Figures 10(a) and 10(b) show the change in $\frac{\bar{p}_A}{p_{t,2}}$ with angle of attack and present a detailed assessment of Reynolds number and afterbody effects. It is seen that

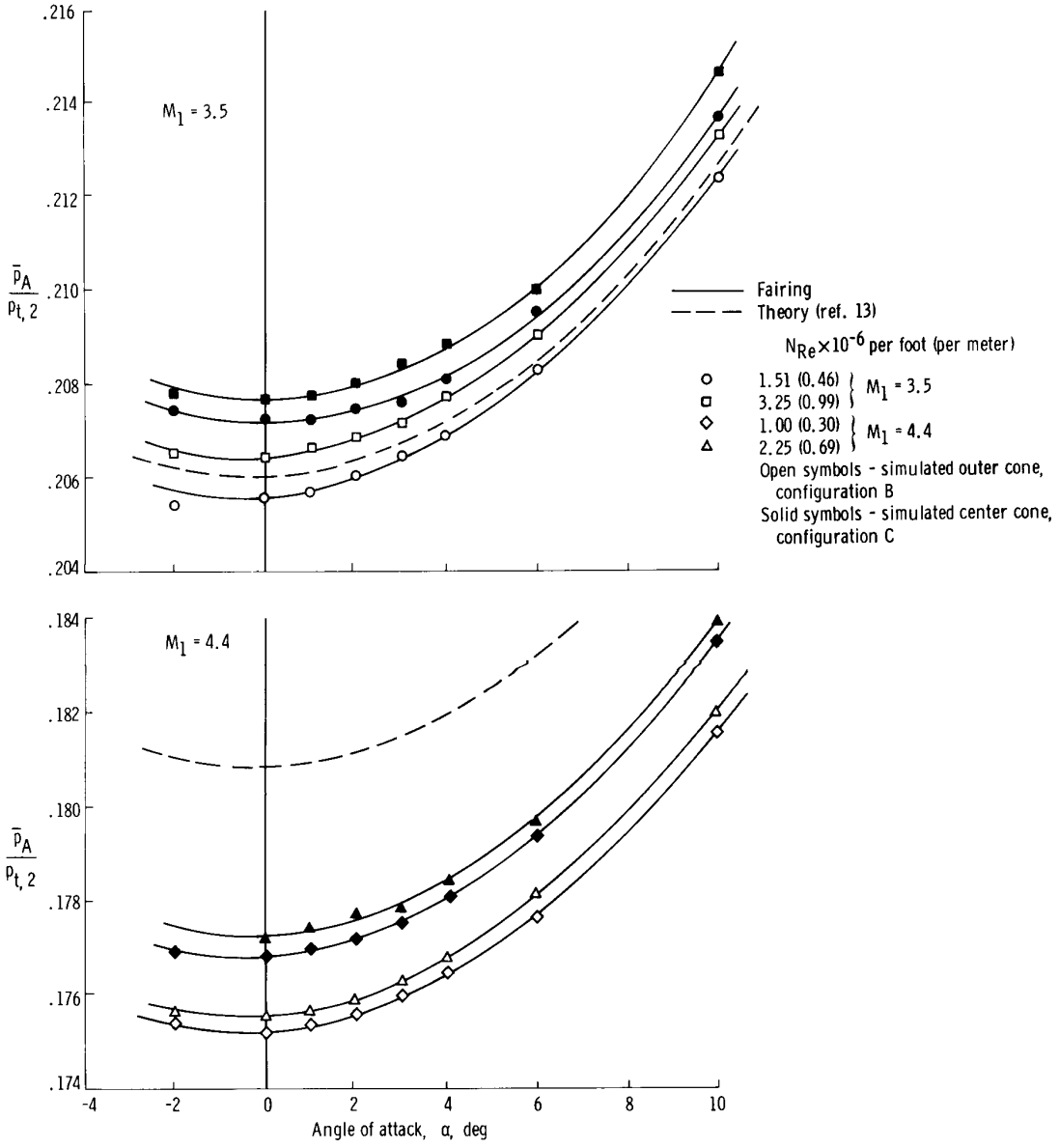

(a) 1- by 3-Foot Supersonic Wind Tunnel.

Figure 10.– Effect of angle of attack on average surface static-to-impact pressure ratio.

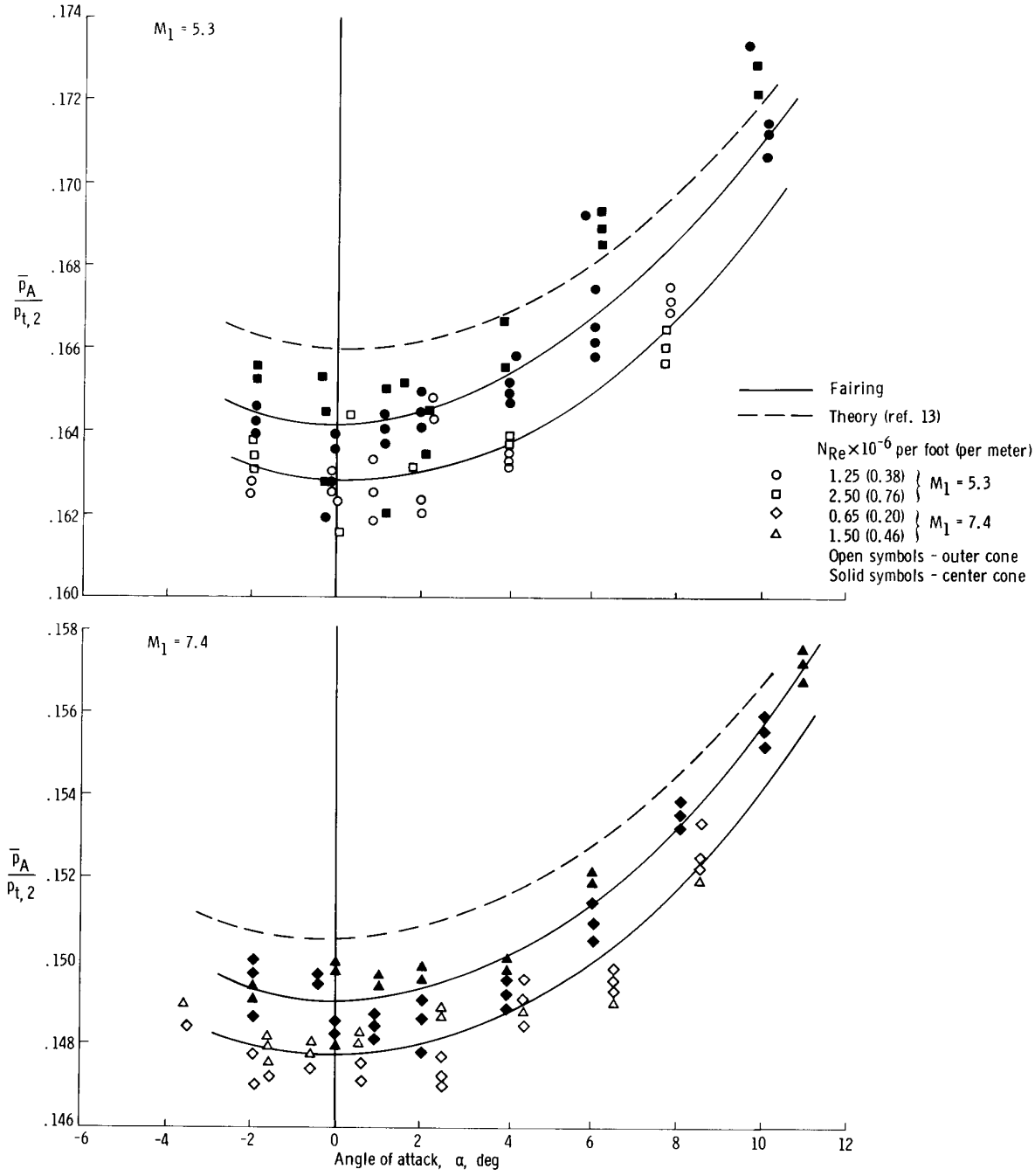

(b) 3.5-Foot Hypersonic Wind Tunnel; configuration A.

Figure 10.– Concluded.

increasing angle of attack results in an increase in $\frac{\bar{p}_A}{p_{t,2}}$ which agrees with the trend of the inviscid sharp-cone-theory curve (ref. 13). The shift in the data away from the theoretical curve at the three higher Mach numbers reflects the previously mentioned reduction in $\frac{\bar{p}_A}{p_{t,2}}$ observed in figure 9. The relatively greater scatter at $M_1 = 5.3$ may be the result of deterioration of the cone surface finish caused by dust from the pebble-bed heater.

At $M_1 = 3.5$ and 4.4 (fig. 10(a)), a definite Reynolds number effect is evident; however, at $M_1 = 5.3$ and 7.4 (fig. 10(b)), the data scatter is such that any trend resulting from Reynolds number is not discernible. The observed increase in $\frac{\bar{p}_A}{p_{t,2}}$ as a result of an increase in Reynolds number is small, amounting to less than a one-third-percent change in Mach number at $M_1 = 3.5$ and 4.4.

The afterbody effect of downstream configuration of the cone on $\frac{\bar{p}_A}{p_{t,2}}$ is more significant than the Reynolds number effect. Figure 10 shows that the $\frac{\bar{p}_A}{p_{t,2}}$ for the center cone (with conical rake adapter) is about 1 percent higher than for the outer cone at the four test Mach numbers. Thus, it is necessary to provide separate calibrations for the center cone (with afterbody) and the outer cone (without afterbody).

It is believed that the effect of the afterbody configuration at the center cone is to increase the pressure within the separated flow region in the cone wake. Evidence of this effect can be seen in figures 11(a) and 11(b), which show shadowgraphs of the

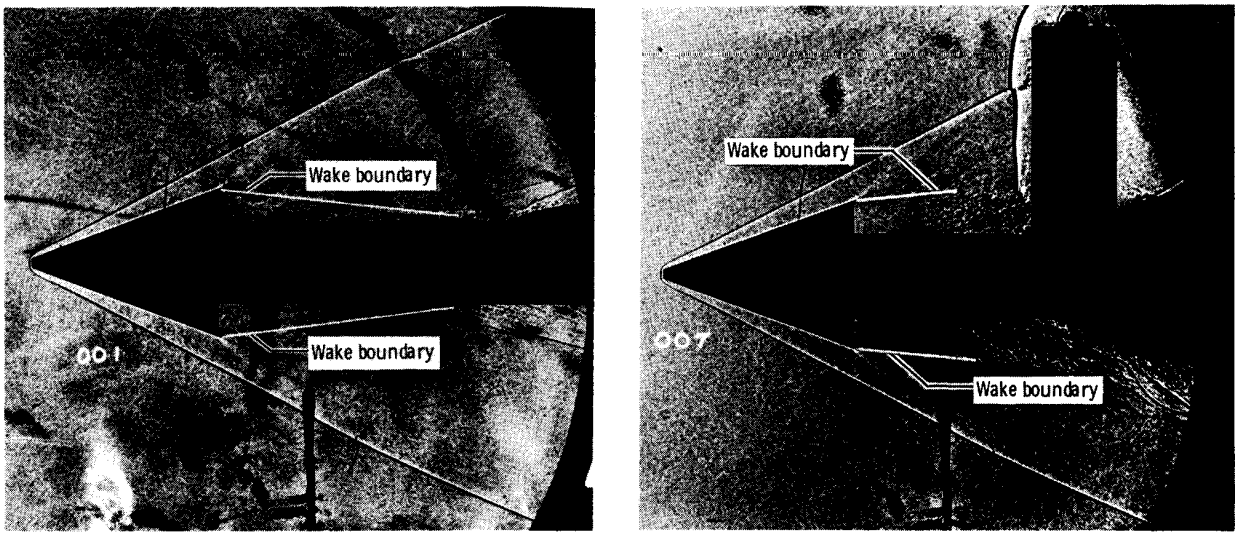

(a) Simulated outer cone, configuration B.

(b) Simulated center cone, configuration C.

Figure 11.—Shadowgraph of cone in 1- by 3-Foot Supersonic Wind Tunnel showing separated cone wake boundary. $M_1 = 3.5$; $\alpha = 0^\circ$; $N_{Re} = 3.25 \times 10^6$ feet (0.99×10^6 meters).

simulated outer cone, configuration B (without afterbody), and the simulated center cone, configuration C (with afterbody), at $M_1 = 3.5$. The boundary of the separated wake is indicated in both figures. The separated-flow region is considerably larger for the simulated center cone than for the simulated outer cone, which indicates a higher wake pressure. This higher wake pressure could then increase the cone surface pressure $\bar{p}_A$, as described previously, through the subsonic portion of the boundary layer.

Figures 12(a) and 12(b) show the effect of angle of attack on the pressure-difference coefficient $\frac{\Delta p}{q_1}$. The results at the four test Mach numbers show good linearity and essentially no effect due to Mach number or Reynolds number. Data scatter was within $\pm 0.1°$ at $M_1 = 3.5$ and 4.4 and within $\pm 0.2°$ at $M_1 = 5.3$ and 7.4. The trend lines pass through zero at $\alpha = 0°$, indicating that the cones were symmetrical. The data agree with theory (ref. 13) at all test conditions.

Data obtained in the 3.5-foot-tunnel tests at $\beta = -2°$ showed no significant difference from the data obtained at $\beta = 0°$. Also, there was no effect due to the ablative simulator bar used on two runs. Consequently, the results can be considered to be independent of a $\pm 2°$ variation in angle of sideslip and independent of the ablative coating on the rake leading edge.

Because the cone calibrations are accurate in Mach number (±2 percent) and flow angularity ($\pm 0.2°$), and nearly independent of Reynolds number over the ranges tested, the cone probe would be useful for the determination of flow-field parameters.

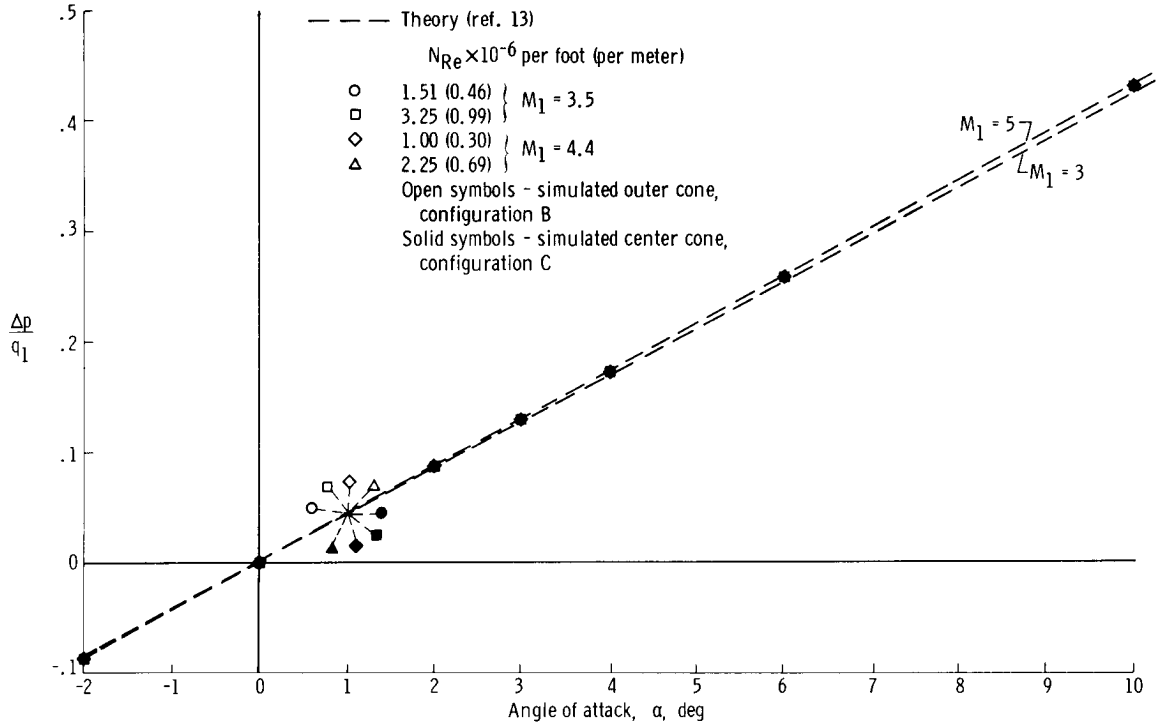

(a) 1- by 3-Foot Supersonic Wind Tunnel.

Figure 12.— Variation of pressure-difference coefficient with angle of attack.

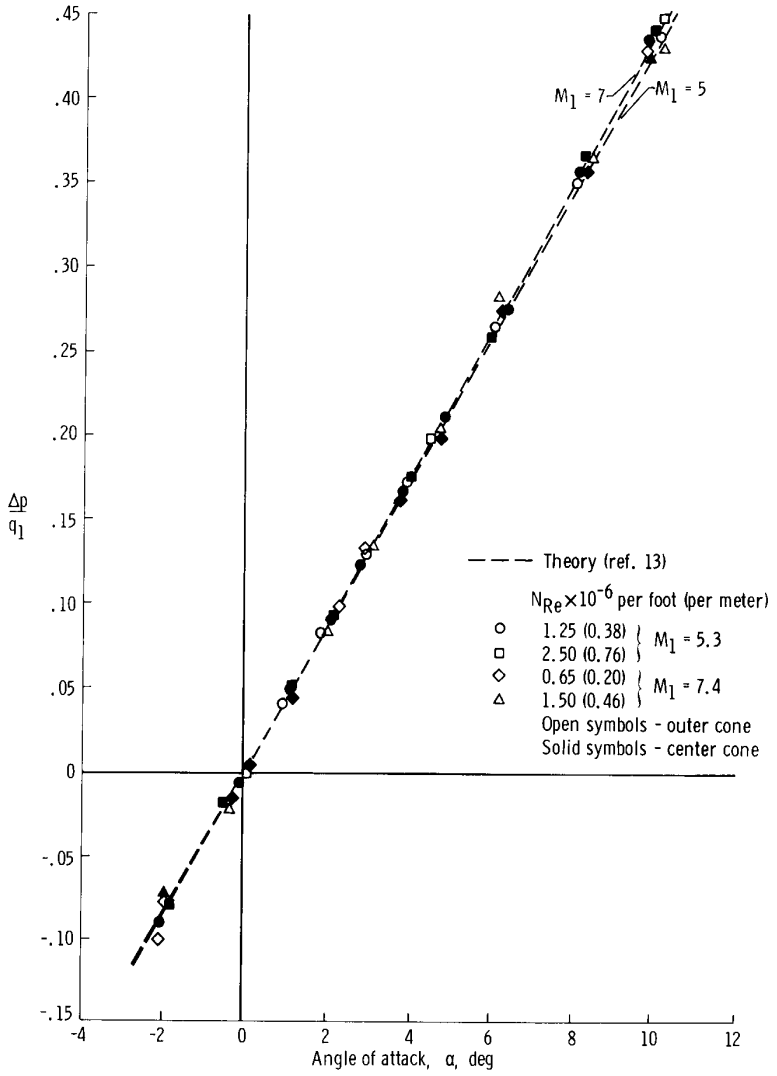

(b) 3.5-Foot Hypersonic Wind Tunnel, configuration A.

Figure 12.– Concluded.

Calibration Equations and Curves

The curves shown in figure 12(a) and 12(b) are essentially linear and independent of Mach number and Reynolds number and can, therefore, be represented by a straight line. The equation form is

$$\alpha \text{ (in degrees)} = \left(\frac{\Delta p}{q_1}\right)_{\alpha} \quad (23.148)$$

Since the cone is symmetrical, the same equation can be used for the angle of sideslip, as follows:

$$\beta\,(\text{in degrees}) = \left(\frac{\Delta p}{q_1}\right)_\beta \quad (23.148)$$

However, it must be noted that the calibration is valid only for small (approximately ±2°) angles of sideslip, if the angle of attack is large. However, if the angle of attack is small (±2°), the calibration should be accurate for angles of sideslip up to ±10°.

Figures 13 and 14 present the final calibration curves for the 40°-cone probes. These curves are valid at least in the Mach/Reynolds number range of tests shown in figure 5. Figure 13 shows Mach number as a function of $\frac{\bar{p}_A}{p_{t,2}}$ at zero angle of attack

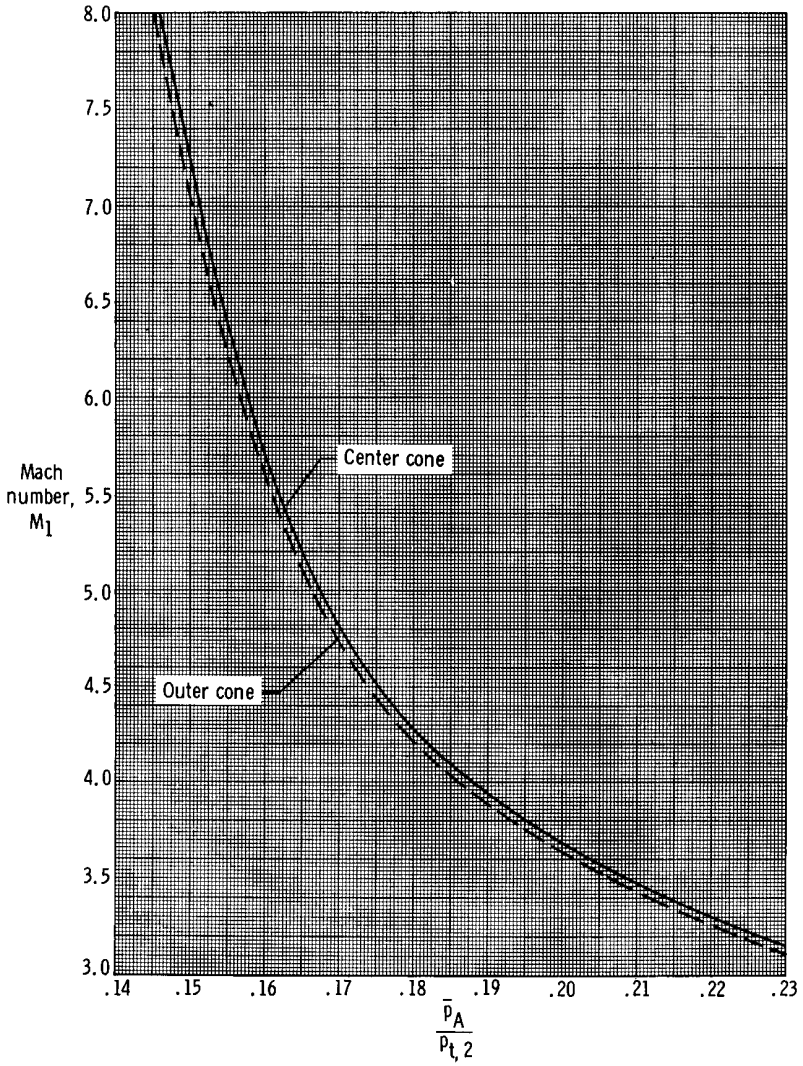

Figure 13.– Final calibration curve showing variation of Mach number with average surface static-to-impact pressure ratio at 0° angle of attack.

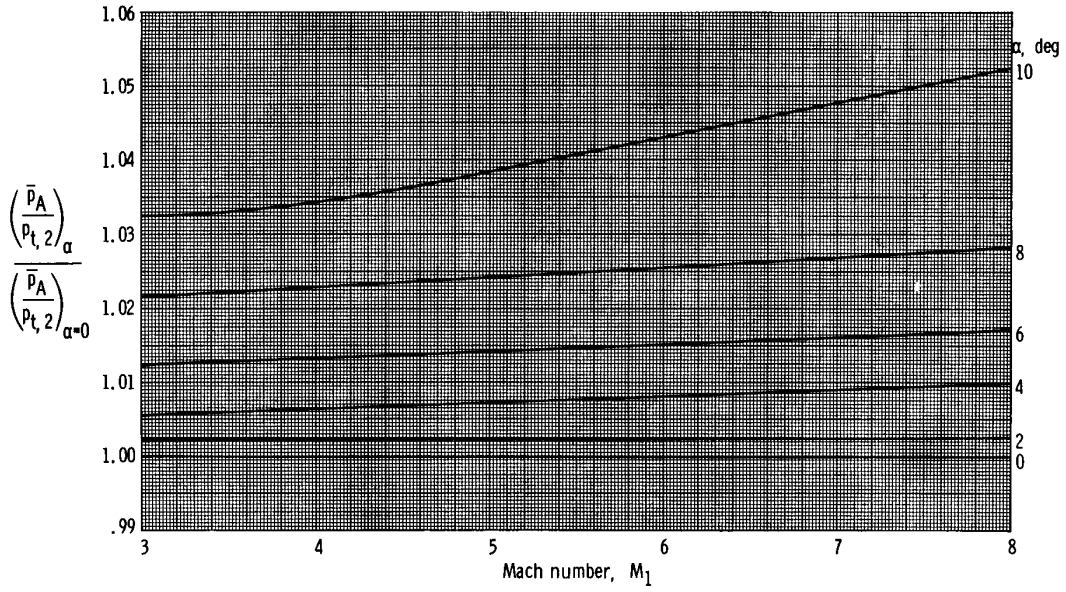

Figure 14.– Final calibration curve showing variation of average surface static-to-impact pressure ratio correction factor with Mach number and angle of attack.

for the center cone and the outer cone. Figure 14 combines the results of figures 10(a) and 10(b). The change in $\frac{\bar{p}_A}{p_{t,2}}$ was divided by the value of $\frac{\bar{p}_A}{p_{t,2}}$ at zero angle of attack to obtain a percentage change in $\frac{\bar{p}_A}{p_{t,2}}$ as a function of Mach number and angle of attack. For low angles of attack, the change in $\frac{\bar{p}_A}{p_{t,2}}$ is very small.

An example of how the cone calibration can be used to convert pressure data to flow-field parameters is presented in the appendix. The method is similar to that used in references 5 and 6, but simpler because small sideslip angles are assumed. An iterative procedure is necessary to obtain accurate results.

CONCLUSIONS

As a result of wind-tunnel tests of a 40° conical pressure probe at Mach numbers of 3.5, 4.4, 5.3, and 7.4, the following conclusions were reached:

1. The estimated accuracy of the calibration curves at a Mach number of 7.4 is ±2 percent in Mach number and ±0.2° in flow angle. At a Mach number of 3.5, the accuracy is ±0.4 percent in Mach number and ±0.1° in flow angularity. Thus, the probe tested could be used to accurately determine local Mach number and flow

angularity over the range covered in the calibration.

2. The calibrated cone surface static-to-impact-pressure ratio $\frac{\bar{p}_A}{p_{t,2}}$ agreed with inviscid sharp-cone theory at a Mach number of approximately 3.5, but was about 2 percent lower than theory for the three higher Mach numbers tested.

3. The pressure-difference coefficient $\frac{\Delta p}{q_1}$ versus angle-of-attack curve was linear, essentially independent of Mach number and Reynolds number, and agreed with theory at the four Mach numbers tested.

4. Reynolds number effects were very small at Mach numbers of 3.5 and 4.4 and were within data scatter at Mach numbers of 5.3 and 7.4 over the range tested.

5. A significant afterbody effect due to the conical rake adapter required separate calibrations for the center and outer cones.

Flight Research Center,
National Aeronautics and Space Administration,
Edwards, Calif., March 8, 1968,
729-00-00-02-24.

APPENDIX

SAMPLE CALCULATION

The following sample calculation illustrates the use of the final calibration curves to determine flow-field parameters. Given the following data for the center cone,

$$p_{t,2} = 1185 \text{ lb/sq ft } (56.74 \text{ kN/m}^2)$$

$$p_{s,a} = 163 \text{ lb/sq ft } (7.80 \text{ kN/m}^2)$$

$$p_{s,b} = 208 \text{ lb/sq ft } (9.96 \text{ kN/m}^2)$$

$$p_{s,c} = 275 \text{ lb/sq ft } (13.16 \text{ kN/m}^2)$$

$$p_{s,d} = 222 \text{ lb/sq ft } (10.63 \text{ kN/m}^2)$$

first calculate the arithmetic mean of the four surface static pressures by using the expression

$$\bar{p}_A = \frac{\left(p_{s,a} + p_{s,b} + p_{s,c} + p_{s,d}\right)}{4} = 217 \text{ lb/sq ft}$$

Then

$$\frac{\bar{p}_A}{p_{t,2}} = \frac{217}{1185} = 0.1831$$

Using figure 13 (solid curve),

$$\frac{\bar{p}_A}{p_{t,2}} = 0.1831 \longrightarrow M_1 = 4.17$$

This Mach number is dependent on the assumption that the cone angle of attack was 0°.

Using compressible flow theory in reference 9,

$$M_1 = 4.17 \longrightarrow \frac{p_{t,2}}{p_{t,1}} = 0.1203$$

and

$$\frac{q_1}{p_{t,1}} = 0.06407$$

So,

$$p_{t,1} = \frac{p_{t,2}}{0.1203} = \frac{1185 \text{ lb/sq ft}}{0.1203} = 9850.4 \text{ lb/sq ft}$$

and

$$q_1 = \left(p_{t,1}\right)(0.06407) = (9850.4)(0.06407) = 631.10 \text{ lb/sq ft}$$

Then

$$\left(\frac{\Delta p}{q_1}\right)_\alpha = \frac{p_{s,c} - p_{s,a}}{q_1} = \frac{275 - 163}{631.1} = 0.1774$$

Using the equation from page 16,

$$\alpha = \left(\frac{\Delta p}{q_1}\right)_\alpha (23.148)$$

then

$$\alpha = (0.1774)(23.148) = 4.106^\circ$$

Since the Mach number calculation assumed $\alpha = 0^\circ$, it must be corrected for $\alpha = 4.106^\circ$ as follows. Using figure 14,

$$M_1 = 4.17 \longrightarrow \frac{\left(\frac{\bar{p}_A}{p_{t,2}}\right)_{\alpha=0}}{\left(\frac{\bar{p}_A}{p_{t,2}}\right)_\alpha} = 1.007$$

So

$$\left(\frac{\bar{p}_A}{p_{t,2}}\right)_\alpha = \frac{\left(\frac{\bar{p}_A}{p_{t,2}}\right)_{\alpha=0}}{1.007} = \frac{0.1831}{1.007} = 0.1818$$

This corrected $\frac{\bar{p}_A}{p_{t,2}}$ is then used to obtain a corrected local Mach number. Again using figure 13,

$$\left(\frac{\bar{p}_A}{p_{t,2}}\right)_\alpha = 0.1818 \longrightarrow \left(M_1\right)_{\text{corrected}} = 4.21$$

Since total pressure and dynamic pressure were calculated for $M_1 = 4.17$, they must be recalculated for the corrected Mach number of 4.21, again using the compressible flow theory in reference 9,

$$M_1 = 4.21 \longrightarrow \frac{p_{t,2}}{p_{t,1}} = 0.1164 \text{ and } \frac{q_1}{p_{t,1}} = 0.0620$$

So

$$p_{t,1} = \frac{p_{t,2}}{0.1164} = \frac{1185}{0.1164} = 10,180 \text{ lb/sq ft}$$

and

$$q_1 = p_{t,1}(0.0620) = (10,180)(0.0620) = 631.16 \text{ lb/sq ft}$$

This value of q_1 would then be used to calculate a new $\frac{\Delta p}{q_1}$ and then a new α. However, the change in q_1 was so small (631.16 from 631.10) that no significant change will result.

Also

$$\left(\frac{\Delta p}{q_1}\right)_\beta = \frac{p_{s,b} - p_{s,d}}{q_1} = \frac{208 - 222}{631.1} = -0.02218$$

Then β can be calculated in the same manner as α. Using the equation on page 17,

$$\beta = \left(\frac{\Delta p}{q_1}\right)_\beta (23.148) = (-0.02218)(23.148) = -0.513^\circ$$

Local static pressure p_1 can also be calculated by using the compressible flow theory of reference 9 as follows:

$$M_1 = 4.21 \longrightarrow \frac{p_1}{p_{t,1}} = 0.004997$$

$$p_1 = p_{t,1}(0.004997)$$

$$p_1 = (10,180)(0.005) = 50.9 \text{ lb/sq ft}$$

The final calculated flow-field parameters are

$$M_1 = 4.21$$

$$p_{t,1} = 10,180 \text{ lb/sq ft } (487.4 \text{ kN/m}^2)$$

$$p_1 = 50.9 \text{ lb/sq ft } (2.437 \text{ kN/m}^2)$$

$$q_1 = 631.1 \text{ lb/sq ft } (30.22 \text{ kN/m}^2)$$

$$\alpha = 4.1^\circ$$

$$\beta = -0.5^\circ$$

REFERENCES

1. Rubert, Kennedy F.: Hypersonic Air-Breathing Propulsion-System Testing on the X-15. Progress of the X-15 Research Airplane Program. NASA SP-90, 1965, pp. 127-132.

2. Montoya, Earl J.; and Palitz, Murray: Wind-Tunnel Investigation of the Flow Field Beneath the Fuselage of the X-15 Airplane at Mach Numbers From 4 to 8. NASA TM X-1469, 1967.

3. Rippey, J.: Flow-Field Investigation of a 0.0667-Scale Model of the X-15 Research Vehicle at Mach 4, 6, and 8. AEDC-TDR-64-201, Arnold Eng. Dev. Center, Oct. 1964.

4. Gallo, William F.; and Rakich, John V.: Investigation of Methods for Predicting Flow in the Shock Layer Over Bodies at Small Angles of Attack. NASA TN D-3946, 1967.

5. Norris, John D.: Calibration of Conical Pressure Probes for Determination of Local Flow Conditions at Mach Numbers From 3 to 6. NASA TN D-3076, 1965.

6. Centolanzi, Frank J.: Characteristics of a 40° Cone for Measuring Mach Number, Total Pressure, and Flow Angles at Supersonic Speeds. NACA TN 3967, 1957.

7. Ray, A. D.: Mach Number 3 to 8 Calibrations of a 30-Deg Conical Probe. AEDC TR-66-168, Arnold Eng. Dev. Center, Sept. 1966.

8. Mechtly, E. A.: The International System of Units - Physical Constants and Conversion Factors. NASA SP-7012, 1964.

9. Ames Research Staff: Equations, Tables, and Charts for Compressible Flow. NACA Rept. 1135, 1953. (Supersedes NACA TN 1428.)

10. Sims, Joseph L.: Tables for Supersonic Flow Around Right Circular Cones at Zero Angle of Attack. NASA SP-3004, 1964.

11. Cleary, Joseph W.: An Experimental and Theoretical Investigation of the Pressure Distribution and Flow Fields of Blunted Cones at Hypersonic Mach Numbers. NASA TN D-2969, 1965.

12. Weiss, R. F.; and Nelson, W.: On the Upstream Influence of the Base Pressure. BSD-TR-67-21 (Res. Rep. 264), Avco Everett Res. Lab., Jan. 1967.

13. Babenko, K. I.; et al.: Three-Dimensional Flow of Ideal Gas Past Smooth Bodies. NASA TT F-380, "Science" Publishing House (Moscow), 1964. (Available from CFSTI, Springfield, Va.)